NRC Publications Archive
Archives des publications du CNRC

Trapping open and closed forms of FitE-A group III periplasmic binding protein

Shi, Rong; Proteau, Ariane; Wagner, John; Cui, Qizhi; Purisima, Enrico O.; Matte, Allan; Cygler, Miroslaw

Trapping open and closed forms of FitE—A group III periplasmic binding protein

Rong Shi,[1] Ariane Proteau,[1] John Wagner,[2] Qizhi Cui,[2] Enrico O. Purisima,[2] Allan Matte,[2] and Miroslaw Cygler[1,2]*

[1] Department of Biochemistry, McGill University, Montréal, Québec, Canada H3G 1Y6

[2] Biotechnology Research Institute, NRC, Montréal, Québec, Canada H4P 2R2

ABSTRACT

Periplasmic binding proteins (PBPs) are essential components of bacterial transport systems, necessary for bacterial growth and survival. The two-domain structures of PBPs are topologically classified into three groups based on the number of crossovers or hinges between the globular domains: group I PBPs have three connections, group II have two, and group III have only one. Although a large number of structures for group I or II PBPs are known, fewer group III PBPs have been structurally characterized. Group I and II PBPs exhibit significant domain motions during transition from the unbound to ligand-bound form, however, no large conformational changes have been observed to date in group III PBPs. We have solved the crystal structure of a periplasmic binding protein FitE, part of an iron transport system, *fit*, recently identified in a clinical *E. coli* isolate. The structure, determined at 1.8 Å resolution, shows that FitE is a group III PBP containing a single α-helix bridging the two domains. Among the individual FitE molecules present in two crystal forms we observed three different conformations (open, closed, intermediate). Our crystallographic and molecular dynamics results strongly support the notion that group III PBPs also adopt the same Venus flytrap mechanism as do groups I and II PBPs. Unlike other group III PBPs, FitE forms dimers both in solution and in the crystals. The putative siderophore binding pocket is lined with arginine residues, suggesting an anionic nature of the iron-containing siderophore.

INTRODUCTION

Iron is indispensable for growth of almost all living organisms and participates in a variety of metabolic and cellular processes.[1] The majority of environmental iron exists in a ferric form (Fe^{3+}), biologically inaccessible due to its low solubility at physiological pH. To sequester iron from their environment under iron-limiting conditions, gram-negative bacteria have evolved a variety of high-affinity iron acquisition systems.[2] One strategy involves the synthesis and secretion of siderophores, small iron-chelating molecules. Ferri-siderophore complexes are taken up via specific outer membrane receptors in a process that is driven by the cytosolic membrane potential and mediated by the energy-transducing TonB-ExbB-ExbD system.[3] Siderophore-binding PBPs, essential for bacterial survival,[4] work as molecular shuttles to transport the ferri-siderophore from the outer membrane receptors to the ABC transporters in the inner membrane, which subsequently deliver the ferri-siderophores to the cytosol. Siderophores have been divided into three major classes according to the functional groups donating oxygen ligands for iron coordination: catecholates (e.g. enterobactin), hydroxamates (e.g. ferrichrome), and α-hydroxy-carboxylates (e.g. staphyloferrin A).[1] Many of the recently discovered siderophores contain chemical features of at least two classes and are therefore classified as "mixed-type" siderophores. *E. coli* K-12 possesses at least six highly specific outer membrane receptors enabling the uptake of eight siderophore complexes, including enterobactin, coprogen, ferrichrome, ferrioxamine, and ferri-dicitrate. In contrast, only three associated periplasmic siderophore binding protein-dependent ABC systems are known, one each for the transport of ferri-citrate, ferri-hydroxamates, and ferri-catechols.[5]

Recently, an additional ABC iron transport system, *fit*, has been identified from a clinical *E. coli* isolate and characterized.[6] Sequence analysis revealed that this iron transport system is also present in many other pathogenic strains and clinical isolates including *E. coli* UT189, APEC strain O1, *E. coli* CFT073, *E. coli* O157:H7 EDL933, and *E. coli*

536, but is not present in the laboratory strain *E. coli* K-12. The *fit* system encodes an outer membrane protein (FitA), a periplasmic binding protein (FitE), two permease proteins (FitC and FitD), an ATPase (FitB), and a protein of unknown function (FitR). Here we investigate the periplasmic binding protein (PBP) of this new iron transport system.

The uptake of solutes into cells is essential for bacterial growth and survival and is performed by a variety of transport systems. Periplasmic binding proteins (PBPs) are essential components of these uptake systems. Bacterial PBPs belong to a diverse protein superfamily[7] that also includes some eukaryotic proteins.[8] PBPs recognize a broad spectrum of ligands[9] and mediate their transport into cells via interaction with a membrane-bound complex or initiate chemotaxis by activating flagellar motion.[10] PBPs may also serve as chaperones for the refolding of denatured proteins.[11]

PBPs have been identified that bind a wide range of ligands, including carbohydrates, amino acids, vitamins, anions, metal ions, metal-chelating complexes, dipeptides, and oligopeptides.[9,12] Accordingly, the proteins within this large family possess diverse sequences and sizes. Although unrelated at the level of primary sequence, almost all PBPs share a common structural motif consisting of two globular domains joined by a hinge region.[8,10] The cleft between the two domains constitutes the ligand binding site. The switch from an open, ligand-free form to a closed, ligand-bound form is achieved through a bending motion around the hinge region(s), commonly termed the "Venus flytrap."[10,13–15]

On the basis of sequence similarities and the chemical nature of the bound ligands, Tam and Saier classified PBPs into eight distinct clusters.[16] Another way of classifying PBPs is based on their topology, according either to the number and topological arrangement of α-helices and β-strands[17,18] or, alternatively, based on the number of crossovers between the two globular domains.[10,19] The latter classification scheme divides PBPs into three groups, characterized by the number of interdomain connections, with group I PBPs having three connections, group II having two, and group III having only one. The structures of many diverse group I and group II PBPs have been determined, but only a few group III PBPs have been structurally characterized. Group III PBPs contain an α-helix connecting the two domains, and include PBPs that bind manganese (PsaA[20] and MntC[21]), zinc (TroA[22,23] and ZnuA[24,25]), ferrichrome (FhuD),[26] vitamin B12 (BtuF),[19,27] enterobactin (CeuE),[28] and heme (ShuT and PhuT).[29] Unlike PBPs from groups I and II, for which significant domain movements upon ligand binding have been observed, the ligand-free and ligand-bound conformations of TroA and BtuF are nearly identical, suggesting that group III PBPs may have more rigid structures than those of group I and II PBPs. However, recent molecular dynamics studies of FhuD and BtuF indicate that these PBPs may be less rigid than envisioned from the crystal structures and may possess a substantial degree of intrinsic domain–domain flexibility.[30,31] The crystal structure of unliganded BtuF complexed to its ABC transporter BtuC/D showed a more open conformation than observed for BtuF alone.[32]

We have determined the crystal structure of the ligand-free periplasmic binding protein FitE. The structure determined at 1.8 Å resolution shows that FitE belongs to group III PBPs. Most importantly, three different conformations were observed among the independent molecules in two crystal forms, indicating that like group I and II PBPs, group III PBPs are also characterized by interdomain flexibility and can undergo large conformational changes even in the absence of the ligand or its receptor. Unlike other group III PBPs, FitE forms dimers both in solution and in the crystal. Molecular dynamics studies were performed to investigate the intrinsic flexibility of this protein.

MATERIALS AND METHODS

Cloning, expression, and purification

A gene encoding FitE lacking its N-terminal 18-residue signal sequence (residues 19-315, NCBI gi: 12517600), from *Escherichia coli* O157:H7 EDL933[33] was cloned into a modified pET15b vector (Novagen), yielding a fusion protein with an N-terminal, tobacco etch virus (TEV) protease-cleavable his-tag and was expressed in *E. coli* BL21(DE3). For the production of selenomethionine (SeMet)-labeled protein, the *E. coli* methionine auxotroph DL41(DE3) was transformed by the plasmid.[34]

An overnight culture of transformed *E. coli* BL21(DE3) or DL41(DE3) was used to inoculate 1L 2YT medium (or LeMaster medium for SeMet-labeled protein) containing 50 μg/mL ampicillin and was grown at 37°C until the absorbance at 600 nm reached 0.6. Protein expression was induced with 100 μM isopropyl 1-thio-β-D-galactopyranoside (IPTG) followed by 16–20 h incubation at 16°C. Cells were harvested by centrifugation (4000g, 4°C, 25 min) and stored at −20°C. The cell pellet was resuspended in 40 mL of lysis buffer (50 mM Tris, pH 8.0, 0.4M NaCl, 5% (v/v) glycerol, 0.5% (v/v) Triton X-100, 20 mM imidazole, pH 8, 1 mM dithiothreitol (DTT)), and the cells were lysed by sonication (10 × 12 s, with 20 s between bursts). Cell debris was removed by ultracentrifugation (100,000g, 45 min, 4°C). The protein supernatant was loaded onto a 1 mL bed volume of Ni-NTA resin (Qiagen, Mississauga ON) equilibrated with lysis buffer. After application of the protein sample, the column was washed with 40 mL of lysis buffer, followed by 40 mL of buffer A (50 mM Tris, pH 8.0, 1.0M NaCl, 5% (v/v) glycerol, 20 mM imidazole, pH 8.0, 1 mM DTT) and 40 mL buffer B (50 mM Tris, pH 8.0, 0.4M NaCl, 5% (v/v) glycerol, 40 mM imidazole, 1 mM DTT). FitE was eluted in buffer B containing 200 mM

imidazole, pH 8.0. The eluted protein was exchanged on a desalting column into 50 mM Tris, pH 8.0, 250 mM NaCl, 0.5 mM EDTA and cleavage of the fusion protein was carried out by adding TEV protease at a ratio of 1:100 (w/w) and incubating at 23°C for 3 h with occasional mixing followed by incubation at 4°C overnight to near complete cleavage. Protease inhibitor cocktail (Sigma P-8849) was added at a ratio of 1:500 (v/v) to stop the cleavage reaction. Uncleaved FitE and TEV-protease were removed by incubating the protein sample with 100 μL washed Ni-NTA resin and the flow-through containing cleaved FitE was collected. Protein purity was determined by SDS-PAGE and ESI-MS (Agilent 1100 series LC/MSD, Agilent Technologies, Palo Alto, CA), both showing only one species with a molecular weight corresponding to that of cleaved FitE. Gel filtration chromatography was performed using a Superdex-75 column (GE Healthcare) calibrated with molecular mass standards (Sigma) and 200 μL protein (8 mg/mL) was loaded on the column. Prior to crystallization, the protein sample was concentrated by ultrafiltration to 16 mg/mL with concomitant exchange of the buffer to 20 mM Tris pH 8.5, 100 mM NaCl, 5% (v/v) glycerol, 5 mM DTT. SeMet-labeled protein was obtained following the same protocol.

Crystallization

Initial crystallization conditions were found by hanging drop vapor diffusion at 21°C using screens from Hampton Research (Aliso Viejo, CA). The best crystals of FitE were obtained by equilibrating 1 μL of protein (16 mg/mL) in buffer (20 mM Tris, pH 8.5, 100 mM NaCl, 5% (v/v) glycerol, 5 mM DTT) mixed with 1 μL of reservoir solution (0.1M Tris pH 7.5, 0.2M MgCl$_2$, 22% (w/v) PEG 3350) over 0.5 mL of reservoir solution. Two crystal forms were obtained from the same conditions but were harvested from different drops. Both crystal forms belong to space group $P2_12_12_1$ and they differ slightly in the unit cell dimensions, with $a = 51.7$, $b = 113.6$, $c = 224.5$ Å for form A crystals and $a = 50.8$, $b = 109.1$, $c = 222.0$ Å for form B crystals. There are four molecules in the asymmetric unit with a V_m of 2.55 or 2.38 Å^3 Da^{-1}, respectively, corresponding to a solvent content of 52% for form A or 48% for form B crystals.[35]. SeMet-labeled protein crystallized under the same conditions. For data collection, crystals were transferred to a reservoir solution supplemented with 15% (v/v) ethylene glycol and flash cooled in a nitrogen stream at 100 K (Oxford Cryosystems, Oxford, UK).

X-ray data collection, structure solution, and refinement

Diffraction data from a SeMet-labeled FitE form A crystal were collected with a Quantum-4 CCD detector (Area Detector Systems Corp., San Diego, CA), at beam-line X8C at the National Synchrotron Light Source, Brookhaven National Laboratory. Data integration and scaling was performed with HKL2000.[36] Initial phases of FitE were determined by single-wavelength anomalous dispersion (SAD) with data collected at the Se peak energy. Eighteen of the 20 expected selenium atoms in the asymmetric unit were located with the program SOLVE[37] using data collected to 2.2 Å resolution yielding phases with a figure of merit 0.40. Phases were subsequently modified using RESOLVE[38] with a more complete data set collected to 2.2 Å at beamline X29, NSLS, BNL. Automated model building with the program RESOVLE resulted in a starting model containing ∼70% of the mainchain atoms and ∼60% of sidechains. The remainder of the model was built manually using the program COOT[39] and refinement was carried out using the program REFMAC5.[40] Neither a s-cutoff nor NCS restraints were used in refinement. In the final rounds of refinement we applied a translation-libration-screw (TLS) model for anisotropic temperature factors, converging to a final R_{work} and R_{free} of 0.187 and 0.245, respectively.

A dataset for a form B crystal was collected to 1.82 Å resolution at beamline X29. The structure was solved by molecular replacement using the program MOLREP[41] using a combination of two independent molecules from the form A structure as a starting model. Difference electron density maps showed the presence of additional atoms, which were modeled as Mg^{2+}, Cl$^-$, or glycerol according to the observed geometry, coordinating atoms, composition of the mother liquor, and refined B-factors. The model was refined to an R_{work} and R_{free} of 0.188 and 0.219, respectively.

In both form A and form B models, the three C-terminal residues (313–315) are not visible in the electron density map and were not modeled. In form A, residues 19–312 are clearly visible in the electron density map. In form B, the first two N-terminal residues (19–20) are less well defined and were modeled only in subunits A and C. Both FitE form A and form B models have good stereochemistry as analyzed using PROCHECK.[42] Final data collection and refinement statistics are shown in Table I. Coordinates have been deposited in the RCSB Protein Data Bank[43] under accession codes 3BE5 and 3BE6, for FitE from crystal form A and B, respectively.

Molecular dynamics simulation

The AMBER 9[44] suite of programs together with the AMBER ff03 force field[45,46] were used to perform molecular dynamics (MD) simulations and trajectory analysis. The starting point for the MD simulations was the closed conformation (conformer 3) of the monomer and a dimer with both molecules in a closed conformation. The protein was solvated in a truncated octahedron TIP3P water box,[47] with the distance between the wall of the box and the closest atom of the solute being 12.0 Å

Table I
X-ray Data Collection and Refinement Statistics

Data set	SAD	Form A	Form B
Data collection			
Space group	$P2_12_12_1$	$P2_12_12_1$	$P2_12_12_1$
a (Å)	51.7	51.7	50.8
b (Å)	113.6	113.6	109.1
c (Å)	224.6	224.5	222.0
Wavelength (Å)	0.9795	1.1	1.1
Resolution (Å)	40–2.20	50–2.20	50–1.82
	(2.28–2.20)	(2.28–2.20)	(1.89–1.82)
Observed hkl	632,645	308,371	464,225
Unique hkl	105,103 (unmerged)	60,135	102,274
Redundancy	6.0	5.1	4.6
Completeness (%)	80.9 (32.1)	87.9 (59.7)^c	92.4 (63.7)
$R_{sym}{}^a$	0.058 (0.192)	0.073 (0.183)	0.081(0.182)
$I/(\sigma I)$	22.7 (5.9)	14.3 (4.8)	13.7 (4.1)
Wilson B (Å^2)		26.4	18.9
$R_{work}{}^b$ (# hkl)		0.187 (57,016)	0.188 (97,076)
$R_{free}{}^b$ (# hkl)		0.245 (3,042)	0.219 (5,120)
B-factors (# atoms;)			
Protein		30.2 (9,060)	20.5 (9,114)
Solvent		33.7 (609)	30.3 (807)
Ligands (others)		35.9 (2)	29.5 (26)
Ramachandran			
Allowed (%)		99.5	99.6
Generous (%)		0.5	0.4
Disallowed (%)		0	0
Rms deviation			
Bonds (Å)		0.011	0.008
Angles (°)		1.3	1.0
PDB code		3BE5	3BE6

$^a R_{sym} = (\sum|I_{obs} - I_{avg}|)/\sum I_{avg}$.
$^b R_{work} = (\sum|F_{obs} - F_{calc}|)/\sum F_{obs}$.
^{c}The completeness to 2.4 Å resolution is 93.7%.

and the closest distance between the solute and solvent atoms is 0.8 Å. Sodium ions were added to neutralize the protein charge. Applying harmonic restraints with force constants of 10 kcal mol^{-1} Å^{-2} to all solute atoms, the energy of the system was minimized first, followed by heating from 100 K to 300 K over 25 ps in the canonical ensemble (NVT) and equilibration for an additional 25 ps to adjust the solvent density under 1 atm pressure in the isothermal isobaric ensemble (NPT) simulation. The harmonic restraints were then gradually reduced to zero with four rounds of 25 ps NPT simulations. After an additional 25 ps simulation, a 20 ns production NPT run was performed with snapshots collected every 1 ps. For all simulations, a 2 fs time-step and 9 Å nonbonded cut-off were used. The Particle Mesh Ewald (PME) method[48] was used to treat long-range electrostatic interactions, and bond lengths involving bonds to hydrogen atoms were constrained by SHAKE.[49]

RESULTS

Monomer structure

The FitE monomer is made of two globular domains strung along a six-turn long α-helix in a clamp-like arrangement [Fig. 1(a)]. The N-terminal domain (residues 19–153) is an α/β/α sandwich. The central seven-stranded β-sheet, with strand order β1-β2-β9-β8-β3-β4-β7, is flanked by two α-helices on either side. Six strands of the β-sheet are parallel and one (β2 is antiparallel to the rest. A short, two-stranded β-hairpin (β5 and β6 and a one turn helix project from one end of the β-sheet. The C-terminal domain (residues 176–312) is also an α/β/α sandwich, and is composed of a five-stranded, highly twisted mixed β-sheet with strand order β12-β11-β10-β13-β14. Two α-helices roughly parallel to the strands are located on one side facing the N-domain and on the other side, there is a three-turn helix, α9, nearly perpendicular to the strands. The domains share structural similarity in their cores and can be superimposed with a root-mean-square deviation (rmsd) of 2.7 Å for 76 Cα atoms. These two domains could have therefore arisen through an ancient gene duplication event. A short loop in the C-domain is constrained by a disulfide bond between Cys268 and Cys274. In form B crystals, for which the data were collected at a high-flux undulator beamline, this disulfide bond is partially broken in all subunits, with the thiol group of Cys274 adopting two conformations. The radiation sensitivity of disulfide bonds has been previously observed in protein crystals.[50,51]

Conformational states of FitE molecules

The four independent molecules in the asymmetric unit are arranged into clearly distinguishable dimers. Comparison of all eight independent molecules in both crystal forms shows that they superimpose with a root mean squares deviation (rmsd) ranging from 0.5 to 2.5 Å for the Cα atoms. Because the rmsd for individual domains is within the range of 0.4–0.75 Å, we conclude that structural changes within the individual domains are small and that the larger rmsd for the entire molecules reflect rigid body movement of the domains relative to one another. In form A crystals, subunits B and D are most similar (rmsd 0.54 Å for 294 Cα atoms) and adopt the conformation which we name conformer 1. Subunit A (rmsd to subunit B of 0.92 Å for 294 Cα atoms) represents conformer 2. Subunit C adopts the most different conformation (conformer 3) (rmsd to subunit B of 2.54 Å for all 294 Cα atoms). Superposition of these conformers reveals that conformer 1 represents an open conformation whereas conformer 3 represents a closed conformation [Fig. 1(b)]. Conformer 2 displays a semi-open conformation, intermediate between the open and closed conformers.

Movement of the N- and C-domains towards each other along the interdomain helix (α6) results in narrowing of the ligand-binding cavity [Fig. 1(b)]. The largest shifts are observed for the residues distal to the interdomain helix α6, with the helix α4 moving as much as
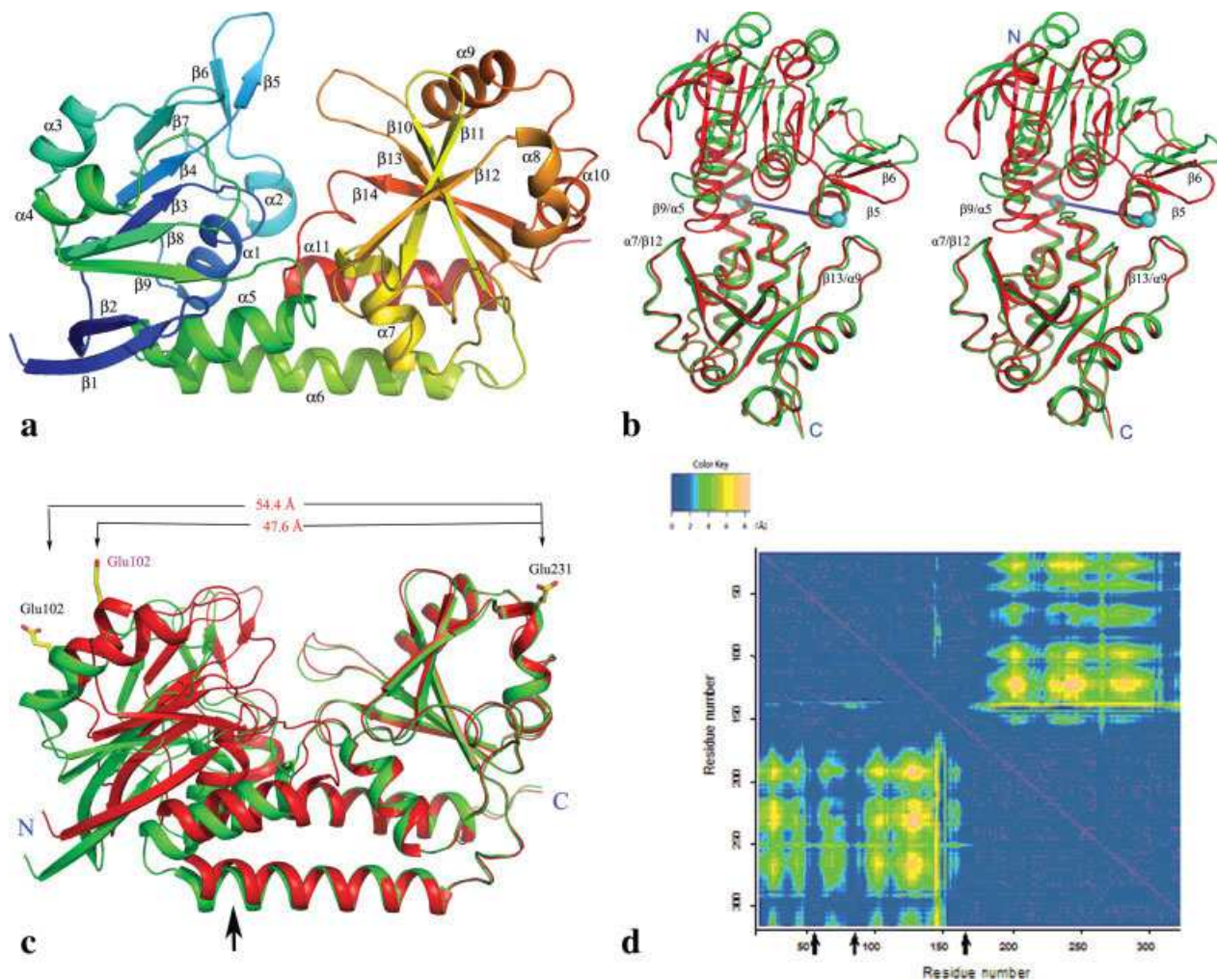
Figure 1

FitE monomer. (**a**) Cartoon representation of the monomer with labeled secondary structures and colored as a rainbow from blue at the N-terminus to red at the C-terminus; (**b**) Domain motion between the open and closed conformers. Superposition of open conformer 1 (green) and closed conformer 3 (red) based on residues in the C-terminal domain. The largest shift is in the regions distal from the interdomain helix α6. The four structural elements forming the gate to the binding cavity are indicated. The thick blue line shows the hinge axis identified by the DynDom server; (**c**) Side view of domain motion between the open (green) and closed (red) conformer. The arrow indicates the hinge within the α6 helix. The Cα distances between Glu102 and Glu231, two residues presumed critical for the recognition of FitE by FitCD, are shown for both conformers. These and subsequent figures were prepared using PyMol (http://pymol.sourceforge.net); (**d**) Cα-Cα difference distance map between the open and closed forms. A Cα-Cα distance matrix was calculated for the open and closed forms, respectively and the absolute value of the difference between the two matrices is displayed as a heat map. The arrows indicate the hinge regions.

~10 Å. Comparison of the three conformers indicates that the opening and closing of the domains can be attributed to small bending of the interdomain helix α6 [Fig. 1(c)]. This bending occurs within the first two turns of helix α6 (residues 156–164). Comparison shows that the α-helical *n*, *n* + 4 backbone hydrogen bonds in the first two turns are ~0.2 Å longer in the closed conformer 3. Analysis of domain–domain motions relating conformers 1 and 3 using the DynDom server (http://fizz.cmp.uea.ac.uk/dyndom/)[52] shows that the opening-closing movement involves an 18.5° rotation of one domain around the hinge axis passing through residues 80–82

and 158–160 [Fig. 1(b)]. These structural changes are summarized quantitatively in a Cα-Cα difference distance map [Fig. 1(d)].Within each domain the relative positions of the Cα atoms change less than 2 Å. On the other hand, between domains, the relative positions of the Cα atoms change by >4 Å. Moreover, the hinge regions are readily identified as those Cα atoms whose relative positions with respect to both domains do not differ much between the closed and open forms. From the distance map, these are seen to be residues 53–58, 78–83 and 153–168.

The conformational state of FitE differs in the relative positioning of regions lining the ligand binding pocket
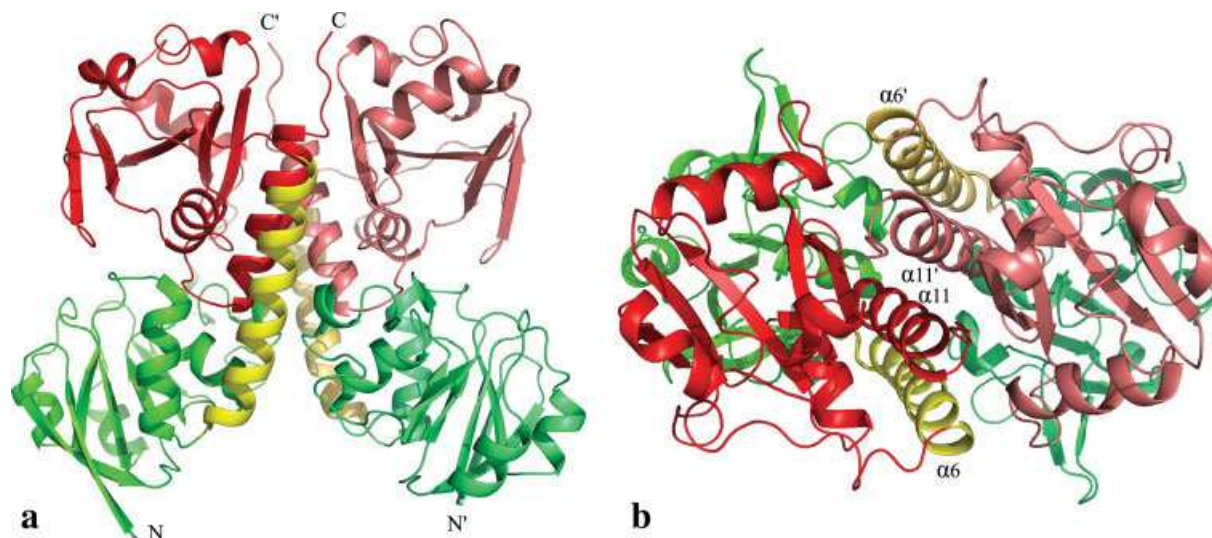
Figure 2

Dimerization of FitE. (**a**) Side view of the FitE dimer, indicating that the major interactions are contributed by the C-domain; (**b**) Top view of the FitE dimer showing four α-helices lining the dimer interface.

[Fig. 1(b)]. The conversion to a closed state is associated with a 2.6 Å shift of loop β9/α5 (residues 136–139) in the N-domain to better accommodate the approaching loop α7/β12 from the C-domain. In the closed conformer 3 these two loops form van der Waals contacts (3.2–4.5 Å) stabilizing one end of the binding cavity. A similar closing mechanism exists on the opposite end of the binding pocket, involving the β5/β6 β-hairpin in the N-domain and the loop β13/α9 in the C-domain. These two structural elements approach each other and lock the other end of the cavity [Fig. 1(b)].

The various dimers observed in FitE crystals are made of subunits that adopt different conformations. Therefore, in form A crystals the AB dimer is made of conformers 1 and 2 whereas the CD dimer is made of conformers 1 and 3. In the form B crystal the AB dimer is made of open conformers 1 whereas the CD dimer contains closed conformers 3.

Structural similarity with other group III PBPs

The overall structure of FitE is similar to those of other group III PBPs characterized by a single α-helical segment bridging the two domains. A search using DALI[53] showed that the most similar structures are FeuA from *Bacillus subtilis* (PDB code 2PHZ), CeuE from *Campylobacter jejuni* (PDB code 2CHU),[28] FhuD from *Escherichia coli* (PDB code 1EFD),[26] BtuF from *Escherichia coli* (PDB code 1N2Z),[19] and a putative periplasmic iron-binding protein from *Thermotoga maritima* (PDB code 2ETV). The rmsd between FitE and these proteins is in the range of 3–4 Å for ∼240 Cα atoms.

Except for the vitamin B12 binding protein BtuF, all of these PBPs are associated with siderophore binding. The sequence identity between FitE and any of these proteins is less than 20%. Several metal-specific PBPs also show topological similarities to FitE, although they are characterized by a much narrower and deeper binding cleft, consistent with their roles in transporting uncomplexed metal ions. Among these are ZnuA from *Escherichia coli* (PDB code 2OSV),[25] MntC from *Synechocystis sp. Pcc* 6803 (PDB code 1XVL),[21] and TroA from *Treponema pallidum* (PDB code 1TOA).[22]

Two structural elements defining in part the putative siderophore binding pocket are unique to FitE, namely the β5-β6 hairpin and an extended gating β13/α9 loop [Fig. 1(b)]. FitE also has an extension at the C-terminus following the last helix α11 plays a pivotal role in dimerization.

A unique mode of FitE dimerization

As shown by size exclusion chromatography, FitE forms dimers in solution with an apparent molecular weight of 62 kD. Well-defined dimers are observed also in the crystal. Such dimerization of PBPs is rare, with the majority of characterized PBPs from all groups being monomers. An example of a dimeric PBP that we are aware of is that of TakP, a periplasmic alpha-keto acid binding protein.[55] Dimerization of FitE occurs through an interface formed mainly by the C-domains (β14, α11, the C-terminal extension and the loop between β13 and α9) and the interdomain helix, α6 [Fig. 2(a)]. The helices from both subunits form a parallel stack [α6, α11, α11′, α6′, Fig. 2(b)]. A short stretch (residues 79–87) from the N-domain also participates in the interface.

Two salt bridges (Arg163…Asp87′ and Asp87…Arg163′) and numerous intersubunit hydrogen bonds are formed at the interface. The total surface area buried upon dimer formation is ~1770 Å^2 per monomer, accounting for 13.5% of the total monomer surface area.

The residues involved in dimerization of FitE are not conserved in its closest structural homologues. We note that all of these proteins lack the segment immediately following α11, which is critical for FitE dimerization. However, a sequence search using BLAST[56] shows that such extensions exist in several putative iron transport PBPs (gi numbers: 145319950, 157084270, 150955499, and 126716795) from other bacteria, suggesting that these proteins may dimerize in a similar manner to that of FitE.

Molecular dynamics of domain movement

To better understand the conformational flexibility of FitE, we performed a 20 ns molecular dynamics (MD) simulation of a monomer and a dimer, starting from the closed conformation (conformer 3). This simulation of the monomer shows a significant conformational change that occurs around 1.3 ns and results in a sharp increase of the rmsd [Fig. 3(a)]. The conformation is relatively stable for the next 8 ns with an average rmsd of 2.3 Å. Around 10.5 ns, another moderate conformation change occurs and then the conformation is relatively stable for the remainder of the simulation with an average rmsd of 2.8 Å. The simulation performed for the dimer shows a somewhat different behavior, with a gradual and more moderate conformational change. The average rmsd over the last 10 ns for the CD dimer is 2.0 Å. These simulations suggest that FitE is less flexible as a dimer than in a monomeric form. Comparison of the MD structures with the starting crystal structures indicates that after 2 ns, the closed conformer 3 in both monomeric and dimeric forms has changed its original conformation toward that of the open conformer 1.

These results show that in the absence of a bound siderophore molecule, FitE tends to adopt the open conformation and that the two lobes in the dimer are not opening as wide as those in the monomer, reflecting a reduced flexibility of the dimer. To further inspect local conformational flexibility, we also calculated local fluctuations of the backbone atoms with respect to the average structure over 20 ns. The interdomain α-helix exhibits very small fluctuations whereas the largest fluctuations are observed for the loops lining the ligand binding pocket [Fig. 3(b)]. In the dimer, motions of the C-domain are significantly reduced compared to that in the monomer, probably because of the restraints imposed on the C-domain upon dimerization.

Putative siderophore binding cavity

The putative siderophore binding pocket of FitE is formed by loops extending from the N-domain on one
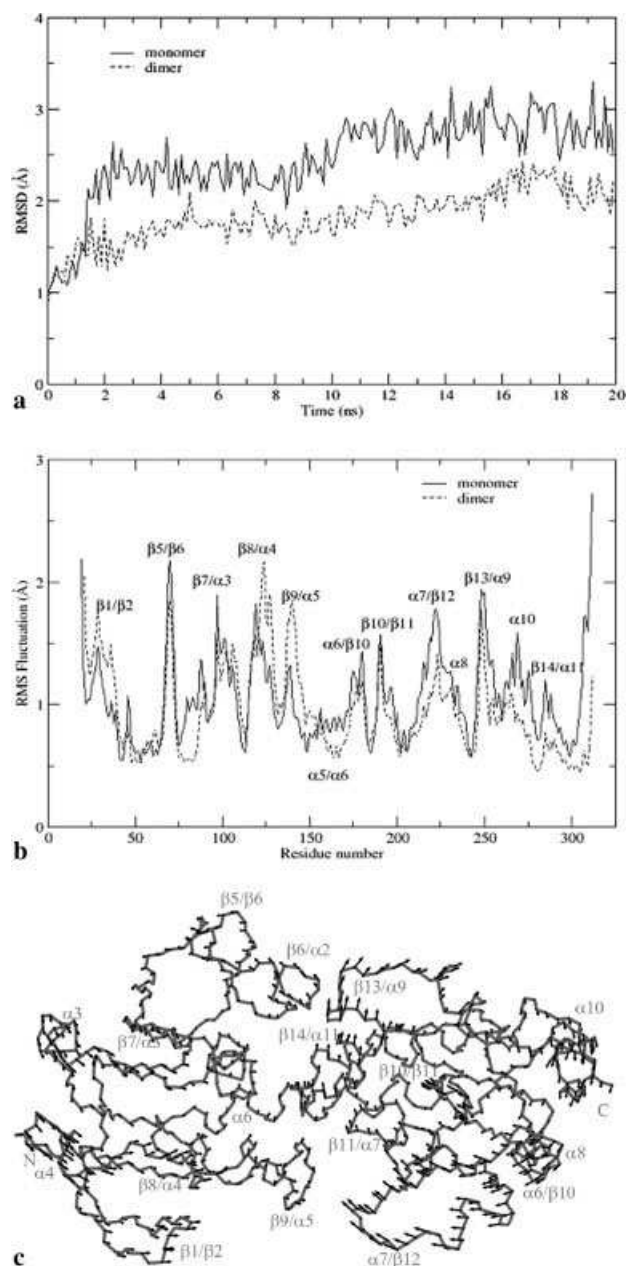
Figure 3

Structural dynamics of FitE monomer and dimer. (**a**) Backbone atom rmsd with respect to the MD starting structure as a function of simulation time. The sampling was done every 100 ps; (**b**) Per residue RMS fluctuation with respect to the MD starting structure over the 20ns simulation; (**c**) Top view of the motion of the monomer backbone atoms along the first mode. Arrows show the directions of the atoms' motion along the mode. The point of an arrow represents the atom's position at the MD trajectory's maximum (most positive) projection and the tail represents the position at the minimum (most negative) projection. Structure and arrows were produced by using the programs VMD[57] and IED.[54]
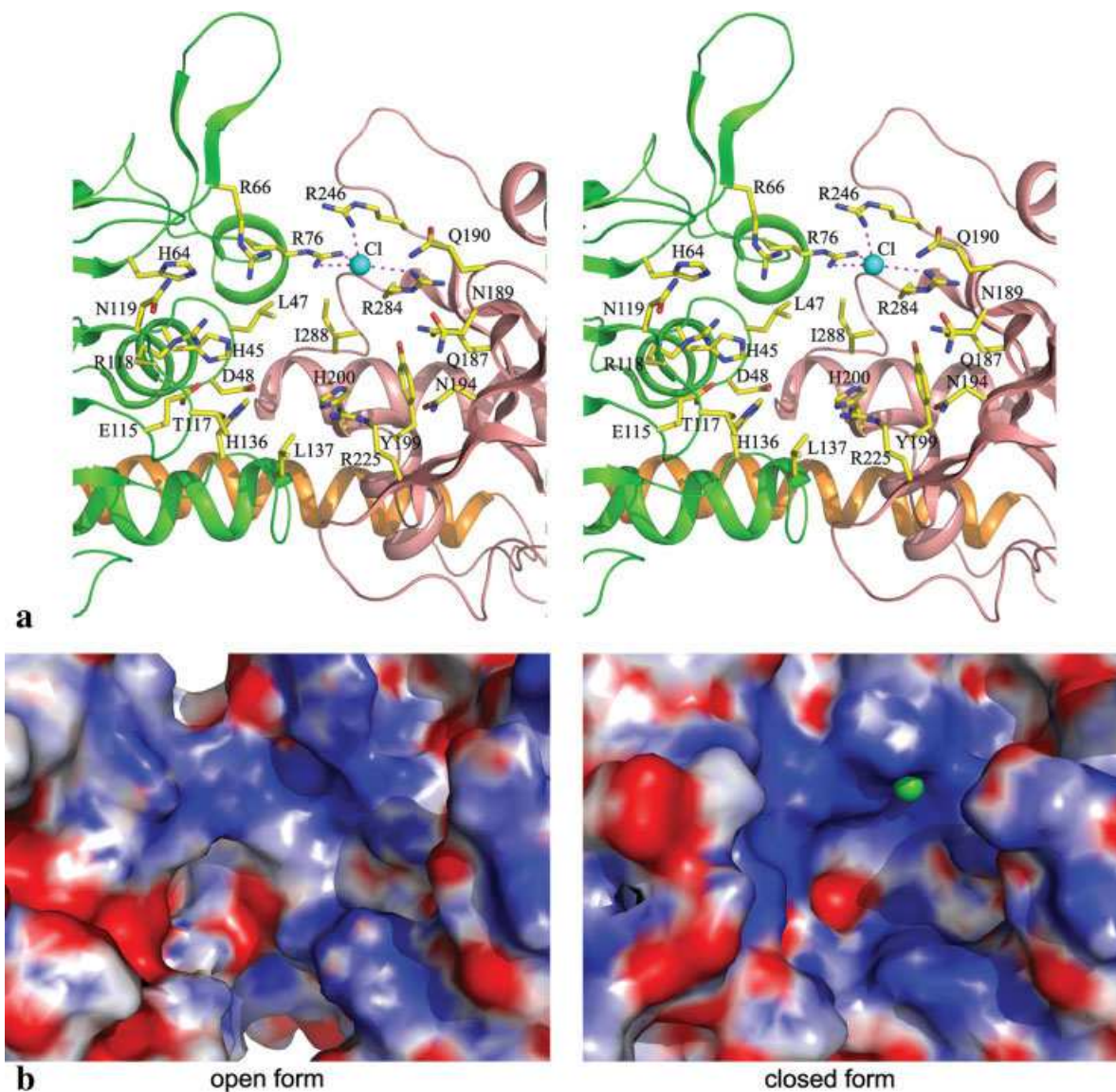
Figure 4

The ligand binding site of FitE. (**a**) Residues lining the binding pocket are shown in standard CPK colors along with surrounding secondary structure elements (N-domain, green; C-domain, salmon). The Cl⁻ ion is shown as a green sphere; (**b**) electrostatic surface potential of the ligand binding site in the open (left) or closed (right) conformation calculated by using APBS.[58] The electrostatic potential is rendered in red and blue to illustrate electrostatically negative and positive regions, respectively, ranging from -10 $k_B T/e$ to $+10$ $k_B T/e$.

side and both the loops and β-strands from the C-domain on the other side. The residues lining the pocket are predominantly hydrophilic, in accordance with the expected characteristics for binding a charged siderophore complex. Although there are few acidic residues, this region contains many basic residues, including six arginines (Arg66, Arg76, Arg118, Arg225, Arg246, and Arg284) and four histidines (His45, His64, His136, and His200) [Fig. 4(a)]. The clustering of positively charged residues at the binding pocket surface [Fig. 4(b)] is a feature of FitE that differentiates it from other group III

PBPs for which structures are available and indicates a different charge characteristic of its ligand as compared to the other PBPs.

Within the putative siderophore-binding pocket of the closed conformer 3, in the vicinity of three arginines, Arg76 from N-domain and Arg246 and Arg284 from C-domain, we have identified a chloride ion [Fig. 4(a)]. In the closed conformation, the guanidinium groups of these three arginines are in close proximity and the presence of a negative charge, for example a chloride ion, is necessary to stabilize this conformation.

DISCUSSION

We have determined the crystal structure of FitE, the PBP of a newly-discovered ABC iron transport system. Despite the absence of the siderophore in the binding pocket, we have observed the ligand-free form of FitE in several conformations: open (conformer 1), intermediate (conformer 2), and closed (conformer 3). This is the first observation of an open-to-closed domain motion in a group III PBP.

Previous structural investigations of group III PBPs in ligand-free and ligand-bound forms showed only very small differences between these two conformations.[19,22,23,26,27,31,59] This contrasted with the large conformational changes observed in group I and II PBPs.[10,60] For example, multiple open structures have been observed for ribose and Leu/Ile/Val binding PBPs, indicating the trajectory of the conformational transition upon ligand binding.[61,62] In the case of the glucose/galactose PBP, it was shown that the closed form could be adopted not only by ligand-bound[63,64] but also by ligand-free protein.[65] The presence of several conformational states for group I and II have also been confirmed by kinetic studies of ligand binding.[66,67]

The small conformational changes observed in all previously studied crystal structures of group III PBPs raised questions regarding how ligand-bound and ligand-free forms are distinguished by the inner membrane ABC transporters associated with group III PBPs. The necessity for selectivity becomes clear if we consider that the number of inner membrane transporters is an order of magnitude lower than that of the PBPs.[5,10] The ability of the membrane transporter to readily distinguish between ligand-loaded and ligand-free states is pivotal to maintain efficient transport at low ligand concentrations, where most PBPs will exist in a ligand-free form.[10] The recent report of the crystal structure of a catalytic intermediate of the maltose transporter suggested that only the closed, ligand-loaded binding protein, not the open apo form, initiates formation of the catalytic transition state.[68] Molecular dynamics simulations of the group III PBPs FhuD and BtuF suggest that they are more flexible than previously assumed from crystallographic studies, and show that additional conformational space is accessible to these proteins.[30,31] The recent crystal structure of the BtuCD-BtuF complex demonstrated that unliganded BtuF bound to the transporter adopted a more open conformation than that observed in BtuF alone, with the insertion of the periplasmic BtuC loops into the vitamin B12 binding pocket.[32] When the N-terminal domain is superposed with that of the isolated BtuF, a ~8° rotation of the C-terminal domain was observed around a hinge located at the C-terminal end of the interdomain helix. The authors suggested that the relative opening of the two lobes of BtuF could be triggered by its docking to BtuCD.

Previous studies suggested that formation of salt bridges between acidic residues of the periplasmic binding proteins and corresponding arginines of the transmembrane protein serve as recognition triggers.[19,69–71] This has been confirmed by the crystal structure of the BtuCD-BtuF complex in which the salt bridge interactions are established between Arg56 from both BtuC subunits of the dimer and Glu72 and Glu202 from BtuF.[32] Structural comparisons and sequence alignments identified Glu102 and Glu231 as their equivalents in FitE, also conserved in other group III PBPs.[19,69–71] On the basis of multiple-sequence alignments (data not shown), the corresponding arginine residues in the transmembrane proteins FitC and FitD are likely Arg56 and Arg78, respectively. The extent of domain movement between the open and closed conformers of FitE can be measured by the distance between the $C\alpha$ atoms of these conserved glutamates. The $C\alpha$ distance between these two glutamate residues in FitE varies from 47.6 Å in the closed state to 54.4 Å in the open conformation [Fig. 1(c)]. The distance of ~47 Å observed in the closed form is likely near the minimum possible value, considering that in this conformer the elements enclosing the binding site are already in van der Waals contact. Similar to other group III PBPs, these two glutamate residues likely play a critical role in the docking of FitE onto its cognate transmembrane proteins FitCD.

The rigid-body motion of the FitE N-domain relative to the C-domain results in a shrinkage of the protein size, roughly represented by a change in the radius of gyration (R_G) The 5.7% reduction in R_G of FitE, as calculated using the program Moleman2[72] of conformer 3 (19.9 Å) when compared with conformer 1 (21.1 Å) is comparable to that of well characterized group I proteins: maltodextrin binding protein, the R_G of which exhibits a ~5.4% reduction upon ligand binding (from 21.8 to 20.7 Å)[60] and leucine/isoleucine/valine-binding protein (LIVBP), which shows a ~4.3% reduction (from 23.2 to 22.2 Å).[73] Therefore, the degree of domain motions during opening or closing for group III periplasmic binding proteins can approximate that exhibited by group I PBPs. To further characterize the domain motions, we also performed essential dynamics (ED) analysis on the MD trajectories of the monomer. The motion of the monomer backbone atoms along the first mode is shown in Figure 3(c). Motions along other modes are very minor. The two domains (lobes) move in opposite directions with a rotational component, which leads to the closed conformations. The N-domain loops ($\beta5/\beta6$, $\beta9/\alpha5$) and the C-domain loops ($\beta13/\alpha9$, $\alpha7/\beta12$) show movement in the opposite directions, which can lock/unlock the binding pocket from each end. These movements are consistent with the structural differences between conformer 1 (open) and conformer 3 (closed) observed in the crystal structures (Fig. 1).

The results in this study are compatible with the previously proposed functional model for PBPs in which the ligand-free PBP exists in a dynamic equilibrium between

open and closed forms, with the equilibrium shifting to the closed conformation upon ligand binding.[30,65,74] As suggested previously, the presence of the closed, unliganded form in the crystal structure proves that at least a small portion of the molecules exist in closed form in solution and can thus be trapped in the crystal lattice.[65] In this regard, our crystallographic and MD results for FitE strongly support the notion that group III PBPs also adopt the same Venus flytrap mechanism as do groups I and II PBPs.

A unique feature of FitE is its behavior as a dimer, both in solution and in the crystal. The detection of four different dimer conformers (1-1, 1-2, 1-3, 3-3) among the FitE structures indicates that the two subunits of the FitE dimer may behave asymmetrically and could exist within the periplasm in several different states (empty-empty, empty-loaded, or loaded-loaded), for example in response to the concentration of its cognate ligand. A recent report on TakP, a periplasmic alpha-keto acid binding protein in the tripartite ATP-independent periplasmic transporter (TRAP), revealed that TakP also forms dimers both in solution and in the crystals. The unexpected dimeric structure of TakP led to postulating a molecular mechanism of solute uptake by this dimeric PBP via a channel that connects the binding sites of the two monomers.[55] Recently it was also suggested that two, or even four, substrate-binding sites may function in the ABC transporter complex and that multiple substrate-binding sites in proximity to the entry site of the translocation pore might enhance the transport capacity.[75] The physiological significance of FitE dimerization remains to be elucidated.

The structure of FitE shows that the ligand binding site has a strikingly hydrophilic nature, which allows us to speculate on the chemical nature of the ligand. We speculate that the position occupied by the chloride ion is the binding site for an anionic group of the FitE cognate siderophore molecule with as yet unknown chemical structure.[6] The Cl^- ion found in the binding pocket likely mimics the interactions of the siderophore molecule with FitE. A similar case was reported for the glucose/galactose receptor where water molecules mimicked the hydrogen bonds of the true ligand.[65] The binding sites of several classes of siderophores have been characterized by crystallography, bound either to a PBP or to an outer membrane receptor. FhuD, a PBP whose binding site is lined predominantly by aromatic and apolar residues, binds hydroxamates such as ferrichrome,[26] coprogen, desferal and albomycin.[59] A catecholate-binding (mecam) PBP, CeuE, has a ligand binding site lined with basic residues.[28] A similar binding site characteristic is present in FeuA, another catecholate (bacillibactin)-binding PBP, although the structure is that of a ligand-free protein (PDB code 2PHZ, unpublished). Superposition of FitE and FeuA, shows that Tyr199 of FitE occupies a position inbetween those of residues Tyr187 and Tyr192

in FeuA. The ligand binding pocket of FitA contains many basic residues and is therefore inconsistent with the binding of hydroxamate-class compounds. This was recently substantiated experimentally and it has also been shown that the *fit* system does not transport enterobactin or ferric-di-citrate.[6] However, other catecholate-type or di-citrate siderophores could conceivably bind to FitE. Further studies will be required to clarify this challenging problem.

ACKNOWLEDGMENTS

REFERENCES

1. Miethke M, Marahiel MA. Siderophore-based iron acquisition and pathogen control. Microbiol Mol Biol Rev 2007;71:413–451.
2. Faraldo-Gomez JD, Sansom MS. Acquisition of siderophores in gram-negative bacteria. Nat Rev Mol Cell Biol 2003;4:105–116.
3. Postle K, Larsen RA. TonB-dependent energy transduction between outer and cytoplasmic membranes. Biometals 2007;20:453–465.
4. Braun V, Braun M. Active transport of iron and siderophore antibiotics. Curr Opin Microbiol 2002;5:194–201.
5. Andrews SC, Robinson AK, Rodriguez-Quinones F. Bacterial iron homeostasis. FEMS Microbiol Rev 2003;27:215–237.
6. Ouyang Z, Isaacson R. Identification and characterization of a novel ABC iron transport system, fit, in *Escherichia coli*. Infect Immun 2006;74:6949–6956.
7. Boos W, Lucht JM. Periplasmic binding protein-dependent ABC transporters. In: Neidhardt FC, editor. *Escherichia coli* and *Salmonella*. Washington, DC: ASM Press; 1996. 1209 p
8. Dwyer MA, Hellinga HW. Periplasmic binding proteins: a versatile superfamily for protein engineering. Curr Opin Struct Biol 2004;14:495–504.
9. Hsiao CD, Sun YJ, Rose J, Wang BC. The crystal structure of glutamine-binding protein from *Escherichia coli*. J Mol Biol 1996;262: 225–242.
10. Quiocho FA, Ledvina PS. Atomic structure and specificity of bacterial periplasmic receptors for active transport and chemotaxis: variation of common themes. Mol Microbiol 1996;20:17–25.
11. Richarme G, Caldas TD. Chaperone properties of the bacterial periplasmic substrate-binding proteins. J Biol Chem 1997;272:15607–15612.
12. Felder CB, Graul RC, Lee AY, Merkle HP, Sadee W. The Venus flytrap of periplasmic binding proteins: an ancient protein module present in multiple drug receptors. AAPS PharmSci 1999;1:E2.
13. Conklin BR, Bourne HR. Homeostatic signals. Marriage of the flytrap and the serpent. Nature 1994;367:22.
14. Mao B, Pear MR, McCammon JA, Quiocho FA. Hinge-bending in L-arabinose-binding protein. The "Venus's-flytrap" model. J Biol Chem 1982;257:1131–1133.
15. Sack JS, Saper MA, Quiocho FA. Periplasmic binding protein structure and function. Refined X-ray structures of the leucine/isoleucine/valine-binding protein and its complex with leucine. J Mol Biol 1989;206:171–191.
16. Tam R, Saier MH, Jr. Structural, functional, and evolutionary relationships among extracellular solute-binding receptors of bacteria. Microbiol Rev 1993;57:320–346.
17. Fukami-Kobayashi K, Tateno Y, Nishikawa K. Domain dislocation: a change of core structure in periplasmic binding proteins in their evolutionary history. J Mol Biol 1999;286:279–290.

18. Newcomer ME, Gilliland GL, Quiocho FA. L-Arabinose-binding protein-sugar complex at 2.4 Å resolution. Stereochemistry and evidence for a structural change. J Biol Chem 1981;256:13213–13217.

19. Borths EL, Locher KP, Lee AT, Rees DC. The structure of *Escherichia coli* BtuF and binding to its cognate ATP binding cassette transporter. Proc Natl Acad Sci USA 2002;99:16642–16647.

20. Lawrence MC, Pilling PA, Epa VC, Berry AM, Ogunniyi AD, Paton JC. The crystal structure of pneumococcal surface antigen PsaA reveals a metal-binding site and a novel structure for a putative ABC-type binding protein. Structure 1998;6:1553–1561.

21. Rukhman V, Anati R, Melamed-Frank M, Adir N. The MntC crystal structure suggests that import of Mn2+ in cyanobacteria is redox controlled. J Mol Biol 2005;348:961–969.

22. Lee YH, Deka RK, Norgard MV, Radolf JD, Hasemann CA. *Treponema pallidum* TroA is a periplasmic zinc-binding protein with a helical backbone. Nat Struct Biol 1999;6:628–633.

23. Lee YH, Dorwart MR, Hazlett KR, Deka RK, Norgard MV, Radolf JD, Hasemann CA. The crystal structure of Zn(II)-free *Treponema pallidum* TroA, a periplasmic metal-binding protein, reveals a closed conformation. J Bacteriol 2002;184:2300–2304.

24. Banerjee S, Wei B, Bhattacharyya-Pakrasi M, Pakrasi HB, Smith TJ. Structural determinants of metal specificity in the zinc transport protein ZnuA from synechocystis 6803. J Mol Biol 2003;333:1061–1069.

25. Li H, Jogl G. Crystal structure of the zinc-binding transport protein ZnuA from *Escherichia coli* reveals an unexpected variation in metal coordination. J Mol Biol 2007;368:1358–1366.

26. Clarke TE, Ku SY, Dougan DR, Vogel HJ, Tari LW. The structure of the ferric siderophore binding protein FhuD complexed with gallichrome. Nat Struct Biol 2000;7:287–291.

27. Karpowich NK, Huang HH, Smith PC, Hunt JF. Crystal structures of the BtuF periplasmic-binding protein for vitamin B12 suggest a functionally important reduction in protein mobility upon ligand binding. J Biol Chem 2003;278:8429–8434.

28. Muller A, Wilkinson AJ, Wilson KS, Duhme-Klair AK. An [{Fe(mecam)}2]6-bridge in the crystal structure of a ferric enterobactin binding protein. Angew Chem Int Ed Engl 2006;45:5132–5136.

29. Ho WW, Li H, Eakanunkul S, Tong Y, Wilks A, Guo M, Poulos TL. Holo- and apo- structures of bacterial periplasmic heme binding proteins. J Biol Chem, in press.

30. Kandt C, Xu Z, Tieleman DP. Opening and closing motions in the periplasmic vitamin B12 binding protein BtuF. Biochemistry 2006;45:13284–13292.

31. Krewulak KD, Shepherd CM, Vogel HJ. Molecular dynamics simulations of the periplasmic ferric-hydroxamate binding protein FhuD. Biometals 2005;18:375–386.

32. Hvorup RN, Goetz BA, Niederer M, Hollenstein K, Perozo E, Locher KP. Asymmetry in the structure of the ABC transporter-binding protein complex BtuCD-BtuF. Science 2007;317:1387–1390.

33. Perna NT, Plunkett GI, Blattner FR, Mau B, Blattner FR. Genome sequence of enterohaemorrhagic *Escherichia coli* O157:H7. Nature 2001;409:529–533.

34. Hendrickson WA, Horton JR, LeMaster DM. Selenomethionyl proteins produced for analysis by multiwavelength anomalous diffraction (MAD): a vehicle for direct determination of three-dimensional structure. EMBO J 1990;9:1665–1672.

35. Matthews BW. Solvent content of protein crystals. J Mol Biol 1968;33:491–497.

36. Otwinowski Z, Minor W. Processing of X-ray diffraction data collected in oscillation mode. Methods Enzymol 1997;276:307–326.

37. Terwilliger TC, Berendzen J. Automated MAD and MIR structure solution. Acta Crystallogr 1999;D55:849–861.

38. Terwilliger TC. Automated structure solution, density modification and model building. Acta Crystallogr D Biol Crystallogr 2002;58:1937–1940.

39. Emsley P, Cowtan K. Coot: model-building tools for molecular graphics. Acta Crystallogr D Biol Crystallogr 2004;60:2126–2132.

40. Murshudov GN, Vagin AA, Lebedev A, Wilson KS, Dodson EJ. Efficient anisotropic refinement of macromolecular structures using FFT. Acta Crystallogr D Biol Crystallogr 1999;55:247–255.

41. Vagin A, Teplyakov A. MOLREP: an automated program for molecular replacement. J Appl Crystallogr 1997;30:1022–1025.

42. Laskowski RA, MacArthur MW, Moss DS, Thornton JM. PROCHECK: a program to check the stereochemical quality of protein structures. J Appl Crystallogr 1993;26:283–291.

43. Berman HM, Westbrook J, Feng Z, Gilliland G, Bhat TN, Weissig H, Shindyalov IN, Bourne PE. The protein data bank. Nucleic Acids Res 2000;28:235–242.

44. Case DA, Cheatham TE, III, Darden T, Gohlke H, Luo R, Merz KM, Jr, Onufriev A, Simmerling C, Wang B, Woods RJ. The Amber biomolecular simulation programs. J Comput Chem 2005;26:1668–1688.

45. Duan Y, Wu C, Chowdhury S, Lee MC, Xiong G, Zhang W, Yang R, Cieplak P, Luo R, Lee T, Caldwell J, Wang J, Kollman P. A point-charge force field for molecular mechanics simulations of proteins based on condensed-phase quantum mechanical calculations. J Comput Chem 2003;24:1999–2012.

46. Lee MC, Duan Y. Distinguish protein decoys by using a scoring function based on a new AMBER force field, short molecular dynamics simulations, and the generalized born solvent model. Proteins 2004;55:620–634.

47. Jorgensen WL, Chandrasekhar J, Madura JD, Impey RW, Klein ML. Comparison of simple potential functions for simulating liquid water. J Chem Phys 1983;79:926–935.

48. Darden T, York D, Pedersen L. Particle mesh Ewald: an N [center-dot] log(N) method for Ewald sums in large systems. J Chem Phys 1993;98:10089–10092.

49. Ryckaert JP, Ciccotti G, Berendsen HJC. Numerical integration of the cartesian equations of motion of a system with constraints: molecular dynamics of n-alkanes. J Comput Phys 1977;23:327–341.

50. Burmeister WP. Structural changes in a cryo-cooled protein crystal owing to radiation damage. Acta Crystallogr D Biol Crystallogr 2000;56:328–341.

51. Weik M, Ravelli RB, Kryger G, McSweeney S, Raves ML, Harel M, Gros P, Silman I, Kroon J, Sussman JL. Specific chemical and structural damage to proteins produced by synchrotron radiation. Proc Natl Acad Sci USA 2000;97:623–628.

52. Hayward S, Berendsen HJ. Systematic analysis of domain motions in proteins from conformational change: new results on citrate synthase and T4 lysozyme. Proteins 1998;30:144–154.

53. Holm L, Sander C. Dali: a network tool for protein structure comparison. Trends Biochem Sci 1995;20:478–480.

54. Mongan J. Interactive essential dynamics. J Comput Aided Mol Des 2004;18:433–436.

55. Gonin S, Arnoux P, Pierru B, Lavergne J, Alonso B, Sabaty M, Pignol D. Crystal structures of an extracytoplasmic solute receptor from a TRAP transporter in its open and closed forms reveal a helix-swapped dimer requiring a cation for alpha-keto acid binding. BMC Struct Biol 2007;7:11.

56. Altschul SF, Madden TL, Schaffer AA, Zhang J, Zhang Z, Miller W, Lipman DJ. Gapped BLAST and PSI-BLAST: a new generation of protein database search programs. Nucleic Acids Res 1997;25:3389–3402.

57. Humphrey W, Dalke A, Schulten K. VMD: visual molecular dynamics. J Mol Graph 1996;14:33–38.

58. Baker NA, Sept D, Joseph S, Holst MJ, McCammon JA. Electrostatics of nanosystems: application to microtubules and the ribosome. Proc Natl Acad Sci USA 2001;98:10037–10041.

59. Clarke TE, Braun V, Winkelmann G, Tari LW, Vogel HJ. X-ray crystallographic structures of the Escherichia coli periplasmic protein FhuD bound to hydroxamate-type siderophores and the antibiotic albomycin. J Biol Chem 2002;277:13966–13972.

60. Sharff AJ, Rodseth LE, Spurlino JC, Quiocho FA. Crystallographic evidence of a large ligand-induced hinge-twist motion between the two domains of the maltodextrin binding protein involved in active transport and chemotaxis. Biochemistry 1992;31:10657–10663.

61. Bjorkman AJ, Mowbray SL. Multiple open forms of ribose-binding protein trace the path of its conformational change. J Mol Biol 1998;279:651–664.

62. Trakhanov S, Vyas NK, Luecke H, Kristensen DM, Ma J, Quiocho FA. Ligand-free and -bound structures of the binding protein (LivJ) of the Escherichia coli ABC leucine/isoleucine/valine transport system: trajectory and dynamics of the interdomain rotation and ligand specificity. Biochemistry 2005;44:6597–6608.

63. Vyas NK, Vyas MN, Quiocho FA. Sugar and signal-transducer binding sites of the Escherichia coli galactose chemoreceptor protein. Science 1988;242:1290–1295.

64. Zou JY, Flocco MM, Mowbray SL. The 1.7 Å refined X-ray structure of the periplasmic glucose/galactose receptor from Salmonella typhimurium. J Mol Biol 1993;233:739–752.

65. Flocco MM, Mowbray SL. The 1.9 Å X-ray structure of a closed unliganded form of the periplasmic glucose/galactose receptor from Salmonella typhimurium. J Biol Chem 1994;269:8931–8936.

66. Ledvina PS, Tsai AL, Wang Z, Koehl E, Quiocho FA. Dominant role of local dipolar interactions in phosphate binding to a receptor cleft with an electronegative charge surface: equilibrium, kinetic, and crystallographic studies. Protein Sci 1998;7:2550–2559.

67. Walmsley AR, Shaw JG, Kelly DJ. Perturbation of the equilibrium between open and closed conformations of the periplasmic C4-dicarboxylate binding protein from Rhodobacter capsulatus. Biochemistry 1992;31:11175–11181.

68. Oldham ML, Khare D, Quiocho FA, Davidson AL, Chen J. Crystal structure of a catalytic intermediate of the maltose transporter. Nature 2007;450:515–521.

69. Braun V, Herrmann C. Docking of the periplasmic FecB binding protein to the FecCD transmembrane proteins in the ferric citrate transport system of Escherichia coli. J Bacteriol 2007;189:6913–6918.

70. Mademidis A, Killmann H, Kraas W, Flechsler I, Jung G, Braun V. ATP-dependent ferric hydroxamate transport system in Escherichia coli: periplasmic FhuD interacts with a periplasmic and with a transmembrane/cytoplasmic region of the integral membrane protein FhuB, as revealed by competitive peptide mapping. Mol Microbiol 1997;26:1109–1123.

71. Sebulsky MT, Shilton BH, Speziali CD, Heinrichs DE. The role of FhuD2 in iron(III)-hydroxamate transport in Staphylococcus aureus. Demonstration that FhuD2 binds iron(III)-hydroxamates but with minimal conformational change and implication of mutations on transport. J Biol Chem 2003;278:49890–49900.

72. Kleywegt GJ. Experimental assessment of differences between related protein crystal structures. Acta Crystallogr D Biol Crystallogr 1999;55:1878–1884.

73. Olah GA, Trakhanov S, Trewhella J, Quiocho FA. Leucine/isoleucine/valine-binding protein contracts upon binding of ligand. J Biol Chem 1993;268:16241–16247.

74. Oh BH, Pandit J, Kang CH, Nikaido K, Gokcen S, Ames GF, Kim SH. Three-dimensional structures of the periplasmic lysine/arginine/ornithine-binding protein with and without a ligand. J Biol Chem 1993;268:11348–11355.

75. van der Heide T, Poolman B. ABC transporters: one, two or four extracytoplasmic substrate-binding sites? EMBO Rep 2002;3:938–943.